



Electrospinning of PVDF nanofibers incorporated cellulose nanocrystals with improved properties

Deniz Aydemir · Eser Sözen · Ismail Borazan · Gökhan Gündüz ·
Esra Ceylan · Sezgin Koray Gulsoy · Ayben Kılıç-Pekgözlü ·
Timucin Bardak

Received: 19 August 2022 / Accepted: 9 November 2022 / Published online: 15 November 2022
© The Author(s), under exclusive licence to Springer Nature B.V. 2022, corrected publication 2022

Abstract Polyvinylidene fluoride (PVDF) nanofibers with cellulose nanocrystals (CNCs) were produced with the electrospinning technique at the CNC loading rates of 0.25, 0.50, 0.75, and 1 wt%. CNCs were obtained with acid hydrolysis of microcrystalline cellulose with 64 wt% sulfuric acid. The material properties of CNCs have been studied with scanning electron microscopy (SEM), transmission electron microscopy, atomic force microscopy, X-ray diffraction (XRD), thermal analysis (TGA), ultraviolet (UV–Vis) spectroscopy, and fourier transform infrared spectroscopy. The PVDF nanofibers with

CNCs were produced by the electrospinning technique. The material characterization of neat PVDF and the PVDF–CNC nanofibers were investigated with XRD, TGA, FT-IR, and morphological properties with SEM. The morphological results showed that CNCs were observed as needle-shaped rods and lengths for CNCs were generally in the range of 25–50 nm and 150–300 nm. The crystallinity and crystal size of CNCs were calculated as 75% and 4.8 nm, respectively. CNCs showed the decomposition stages at 100–250 °C and 300–375 °C for the evaporation of the water and decomposition reactions of cellulose, respectively. CNCs exhibited a weak absorbance at 265 nm according to the UV–Vis. As seen in the results of the nanofibers, it was found that CNCs generally decreased the diameters of the nanofibers obtained with the electrospinning when the loading rates of CNCs were raised. The presence of CNCs generally improved the thermal stability of the nanofibers. XRD results showed that crystallinity generally increased with adding CNCs. In FT-IR spectra, any difference was not detected among the PVDF–CNC nanofiber spectra.

D. Aydemir (✉) · E. Sözen · E. Ceylan · S. K. Gulsoy ·
A. Kılıç-Pekgözlü
Department of Forest Industrial Engineering, Faculty
of Forestry, Bartın University, 74100 Bartın, Turkey
e-mail: denizaydemir@bartin.edu.tr

I. Borazan
Department of Textile Engineering, Faculty
of Engineering, Bartın University, 74100 Bartın, Turkey

I. Borazan
Department of Polymer Materials Engineering, Bursa
Technical University, 16310 Bursa, Turkey

G. Gündüz
Department of Industrial Engineering, Faculty
of Engineering and Natural Sciences, Iskenderun
Technical University, 31200 Iskenderun, Hatay, Turkey

T. Bardak
Department of Furniture and Design, Vocational School,
Bartın University, 74100 Bartın, Turkey

Keywords Electrospun nanofibers · Renewable nanomaterials · Polyvinylidene fluoride (PVDF) · Cellulose nanocrystals

Introduction

PVDF has been commonly used in many applications because of its numerous advantages including piezoelectric, pyroelectric, and ferroelectric properties. PVDF, which is a thermoplastic polymer, has the desired properties such as low cost, flexibility, easy processing, and biocompatibility. These advantages make PVDF a good raw material for fiber production in the textile industry (Dodds et al. 2012; Mokhtari et al. 2016). Although there are several fiber production methods e.g. solution spinning, melt spinning, and gel spinning is an easy method for obtaining micro and nano-sized fibers (Huang et al. 2003; Damaraju et al. 2013; Lolla et al. 2018). The electrical forces drive the electrospinning process on the inside or surface of the solution. The free ions in the solution move in response to the electrical field and provide a force to the solution (Reneker et al. 2000). When the electrically charged forces exceed the surface tension force, a liquid jet is ejected from the surface of the solution (Katta et al. 2004). The electrospinning technique has been used for different polymers (e.g. polyvinyl alcohol, polymethyl methacrylate, polyethylene) in fiber production and is an effective method to produce textile fiber from PVDF and industrial fiber including cellulose, cotton, linen, etc. (Yarin et al. 2005). With this mechanism, the fibers were dispersed into the nanofibers via the electrospinning process (Reneker et al. 2000; Yee et al. 2007; Xin et al. 2018) and the cellulosic fillers to PVDF can provide enhanced mechanical properties and small-fiber dimension (Sanders et al. 2019).

Cellulose, which is a biopolymer obtained from renewable materials is a value-added material and has major advantages including environmental-friendly, abundant, easy processing, low cost, lightweight, etc. New types of cellulose, such as microfibril cellulose (MFC), cellulose nanofibrils (CNFs), and cellulose nanocrystals (CNCs), can be prepared with the diversification of nano-sized materials. The obtained nano-sized cellulose is a high-performance additive, which is commonly used as a reinforcing agent, rheological modifier, and additive in various high-performance products and applications (Kalia et al. 2011; Aydemir and Gardner 2020a, b; Lee et al. 2021).

PVDF can be influenced by the presence of cellulosic nanoparticles, which affect the crystallization behavior (Mago et al. 2008) and the status

can improve the dimension and properties of the obtained fibers. Some scientific studies showed that the reinforcing of PVDF with several bio-fillers improved the properties of the obtained fibers (Alhassan et al. 2018). As a typical bio-filler, cellulose is a well-known fiber to be utilized in the textile industry for reinforcing purposes (Akduman 2021). Zhang et al. (2015) added the CNCs to PVDF with dimethylformamide (DMF) solution and PVDF–CNC nanocomposites were prepared. The obtained results showed that the incorporation of CNCs improved the thermal and mechanical properties of neat PVDF. In a study, Sheikh et al. (2019) added cellulose acetate (CA) to PVDF, and PVDF–CNC nanofibers were prepared with an electrospinning technique. According to the obtained results, the presence of CA in neat PVDF was found to improve the nanofiber structure. For the same purpose, Wang et al. (2019) studied the CNC effects on the properties of the PVDF nanofibers via an electrospinning process and the obtained results demonstrated that the adding CNCs to PVDF improved the microstructure of the obtained nanofibers. Akduman (2021) studied CA–PVDF nanofiber mats for N95 respirators, and the results showed that the addition of CA to PVDF decreased the dimension of PVDF–CA nanofibers. Various studies were conducted on the electrospinning PVDF nanofibers with CNC (Fashandi et al. 2016; Fu et al. 2017; Rincón-Iglesias et al. 2020; Lee et al. 2021), titanium nanotube (Victor et al. 2021), nickel nanoparticle (Sheikh et al. 2011) and silver nanoparticle (Swamidoss et al. 2019; Martin et al. 2019; Zeng et al. 2021).

To the best of the authors' knowledge, most studies were conducted on the fiber properties of PVDF–CNCs at high loading rates including 1, 3, 4 and 5% with the electrospinning method (Fashandi et al. 2016; Fu et al. 2017; Wang et al. 2019) and the obtained results showed that when the loading rate of CNCs used above 1%, many agglomerations may generally appear because of the clumping tendency of free hydroxyl groups in CNCs and therefore, if the high loading rate of CNCs used, the reinforcing effect of CNCs may not appear. As a result, there is a lack of information related to electrospinning fibers of PVDF and CNCs at low loading rates in the literature. In this study, the effects of the low loading rate including 0.25, 0.50, 0.75, and 1% on the properties

of CNC–PVDF nanofibers produced with the electrospinning technique were investigated, and material characterization of the nanofiber mats was conducted.

Materials and methods

Materials

PVDF granules (NSB Polymers Co., Ltd., Turkey, Average Mw~1,000,000) were dried in an oven at 50 °C for a day. Microcrystalline cellulose (CAS Number: 9004-34-6, Sigma Aldrich, Germany) was used as the raw material in the production of CNCs with hydrolyzing reaction [sulfuric acid (98 wt%)] (Istanbul, Türkiye). The other chemicals including dimethylformamide (DMF) and ethanol were purchased from Merck (Istanbul, Turkey). In all experimental analyses, deionized water was used.

Preparation of cellulose nanocrystals

MCC was treated using a 64 wt% aqueous solution of sulfuric acid in a magnetic mixer at 45 °C for 90 min. Ten folds of deionized water were added to the mixture to stop hydrolysis and then keep in the refrigerator for a day. The suspension was centrifuged at 8000 rpm for 20 min (NF 800/800R

centrifuge, Nuve Co., Istanbul, Türkiye) and the supernatant was removed. The centrifuge process was repeated many times until CNCs were turbid in water, and then the CNC solution was taken and placed into dialysis bags for a week until the pH of the water had neutral (Bondeson et al. 2006; Li et al. 2018). Finally, the CNCs were lyophilized with a freeze-dryer (VaCo 2, RotaLab Co., Istanbul, Türkiye) for 2 days. Figure 1 shows procedures to prepare CNC nanomaterials with MCC particles.

Electrospinning of nanofibers

CNCs were first dispersed in DMF in an ultrasonic bath for 15 min, afterwards 15% (weight ratio) PVDF was added into CNC/DMF solution and stirred overnight to dissolve properly. CNC–PVDF solution was filled into a syringe and then loaded in the NanoYarn Spinner (Inovenso Co. Ltd.), and high voltage (15 kV) was applied to the tip of a needle that connected to the syringe. The syringe was pumped with a constant rate of 1 mL/h and the polymer was collected as a nanofibers mat on an aluminum foil placed on the grounded collector. The distance between the needle and collector was 15 cm. The Electrospun device and its elements are shown in Fig. 2.

Fig. 1 The process to obtain CNC nanomaterials with MCC

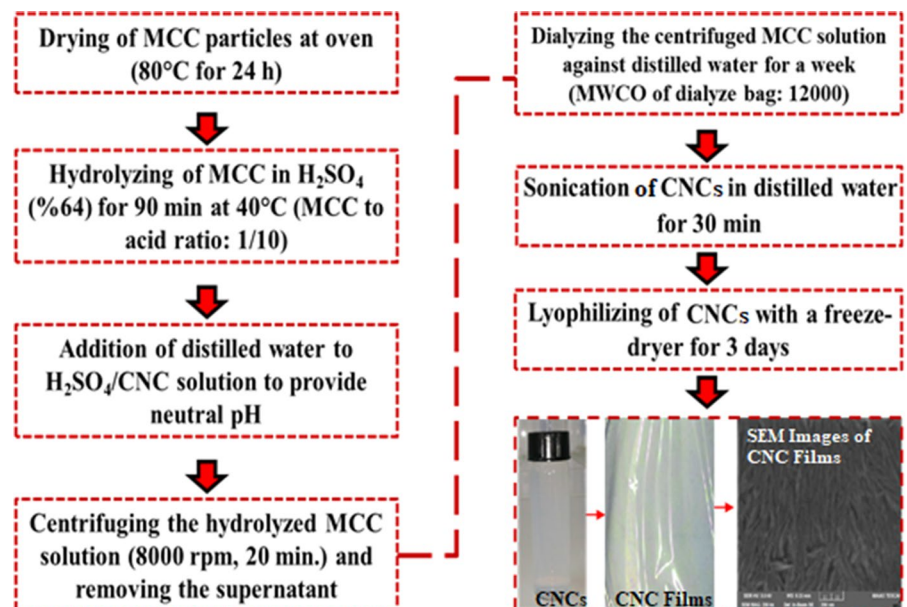
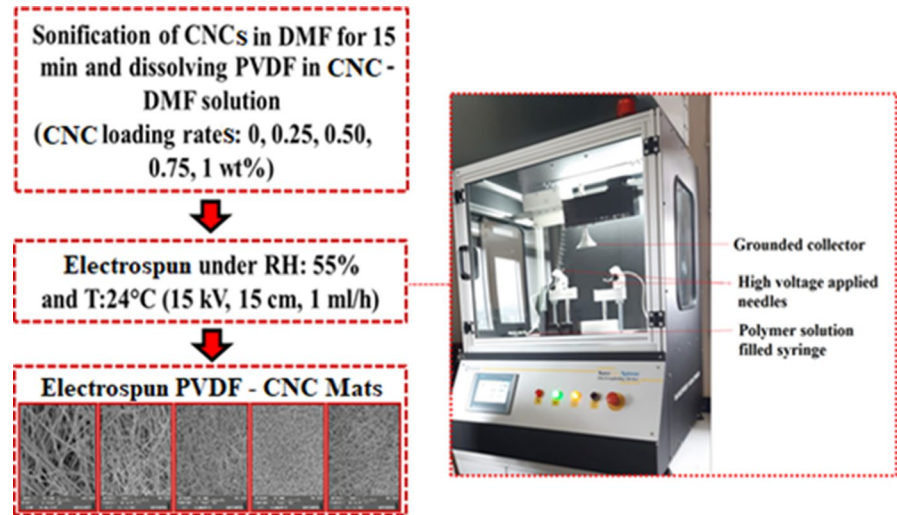


Fig. 2 Electrospinning procedures to prepare the PVDF/CNC nanofibers obtained from PVDF–CNC solution



Characterization

Scanning electron microscopy

Morphological investigations of the samples were conducted with Tescan MAIA3 XMU scanning electron microscopy (Brno, Czech Republic). The samples were coated with a mixture of Palladium/Gold particles to enhance flowing of the electron.

Transmission electron microscopy

TEM investigations of the PCVDF nanofibers were conducted with transmission electron microscopy (Hitachi HighTech HT7700, Chiyoda, Tokyo, Japan). CNC solution was dropped onto a grid and dried in an oven prior to imaging at an accelerating voltage of 100 kV and all the investigations were carried out at $\times 4000$ – $\times 600,000$ HR mode.

Atomic force microscopy

The AFM investigations were conducted with Hitachi 5100 N from 150 to 5 μm . CNC suspension drop was put onto a mica surface, and the mica surface was dried in an oven. The images of CNCs were taken with AFM at 24 °C in the dynamic mode with a scan

rate of 1 Hz and using Si tips with a curvature radius of less than 10 nm.

X-ray diffraction analysis

XRD was conducted with an X-ray diffractometer (Model XPert PRO, Philips PANalytical, Netherlands) with Ni-filtered Cu $K\alpha$ (1.540562 Å) radiation source at a range from 5° to 40° 2 θ range. A silicon zero-background plate was used to make sure there was no peak associated with the sample holder. The crystallinity index (CI) and crystalline size of neat PVDF and the CNC–PVDF nanofibers were calculated by using the formulation given below:

$$CI_{(\%)} = \frac{\sum A_c}{\sum (A_c + A_a)}$$

where A_c is the integrated area underneath the respective crystalline peaks, and A_a is the integrated area of the amorphous halo.

$$D = \frac{K \cdot \lambda}{\beta \cdot \cos(\theta)}$$

where D is the mean length of the crystallite perpendicular to the planes (nm), K is a Scherrer parameter, λ is the wavelength of radiation (0.15406 nm), β is either the integral breadth or the breadth at half maximum intensity in radians and θ is the Bragg angle for the reflection concerned.

Thermogravimetric analysis

Thermal analysis of neat PVDF and the CNC–PVDF nanofibers was carried out with Hitachi STA 7300 TG–DTA analyzer (Chiyoda, Tokyo) on samples of about 5–10 mg samples under the flow of nitrogen at 20 mL/min. The samples were heated from room temperature to 700 °C at 20 °C/min of heating rate. Derivative thermal gravimetry (DTG), weight loss (WL), and temperatures for WL at 10% ($T_{10\%}$), 50% ($T_{50\%}$), and 85% ($T_{85\%}$) were measured according to the TG curves. Derivative thermal analysis (DTA) is a thermoanalytical technique that is similar to differential scanning calorimetry (DSC) and the temperatures including melting (T_m) and degradation (T_d) were calculated from DTA curves.

Ultraviolet spectroscopy

To determine the photocatalytic effect of the CNC in the distilled water, UV analysis was performed with Shimadzu UV 3600 Plus (Shimadzu, Kyoto, Japan) UV–Vis spectrometer in transmission mode at a wavelength range of 200–800 nm under 340 nm wavelength and 0.95 Wm²/nm light source according to ASTM D5208-14 (2020) standard. The UV–Vis spectrometer was set in absorbance mode at the wavelength between 200 and 800 nm range and measurements were conducted on glass plates. Three replicates were made for all specimens and the average of the obtained data was used in the study.

Fourier transform infrared spectroscopy

The FTIR-ATR analysis was carried out with a Shimadzu IRAffinity-1 spectrometer equipped with a single reflection ATR pike MIRacle sampling accessory. Four accumulated spectra with a resolution of 4 cm⁻¹ were obtained for wavenumbers from 800 to 4000 cm⁻¹ with 32 scans for each sample.

Physical properties of obtained mats

Grammage (G) is defined as the mass per unit area of each test specimen. M is the mass and A is the area of

the test specimen, and the Grammage unit is grams per square meter (g/m²) as shown below;

$$G = \frac{K \cdot M}{A}$$

The thickness of each specimen was measured with a caliper and it was shown as μm. The burst index (TAPPI T 403) and air permeability (ISO 5636-3) of each specimen were measured according to relevant standard methods.

Results and discussion

The SEM, TEM, and AFM images of CNCs were shown in Fig. 3. In Fig. 3a and b, CNC was observed as needle-shaped rods with smooth surfaces, and the dispersion of CNCs generally was to be uniform. The morphology of CNCs depends on the source of raw material and the conditions of acid hydrolysis. Reddy and Rhim (2014) have observed similar types of spherical forms of CNCs obtained from garlic skin. In another study, it was found that CNCs prepared from wood dust with acid hydrolysis generally were stiff and rode-like shapes (Shaheen and Emam 2018). The nano-scaled crystals are hard to easily detect by SEM analysis. Therefore, TEM was used to detect the size of the CNC as given in Fig. 3c and d.

It was determined that the diameter and length for CNCs generally were in the range of 25–50 nm and 150–300 nm according to TEM results. To confirm the results, the surface topography of CNCs on a 3D scale was investigated with an AFM probe using non-contact mode. The surface images of CNCs were given in Fig. 3e and f. AFM results showed that CNCs had a rough surface due to the crystal diameters with different heights of the CNCs. The needle-like shaped CNCs were observed. Figure 4 shows the XRD, TGA/DTG, UV–Vis, and FTIR graphs of CNCs.

The XRD pattern of CNCs exhibited three peaks at 16.5°, 22.6°, and 34.5° as given in Fig. 4a. According to the crystallinity calculations, the crystallinity and crystal size of CNCs were calculated as 75% and 4.8 nm. The thermal behavior of the CNCs was given in Fig. 3b. CNCs exhibited at the decomposition stage at 100–250 °C and 300–375 °C for the evaporation of the water and decomposition reactions of cellulose. The temperature at 10, 50,

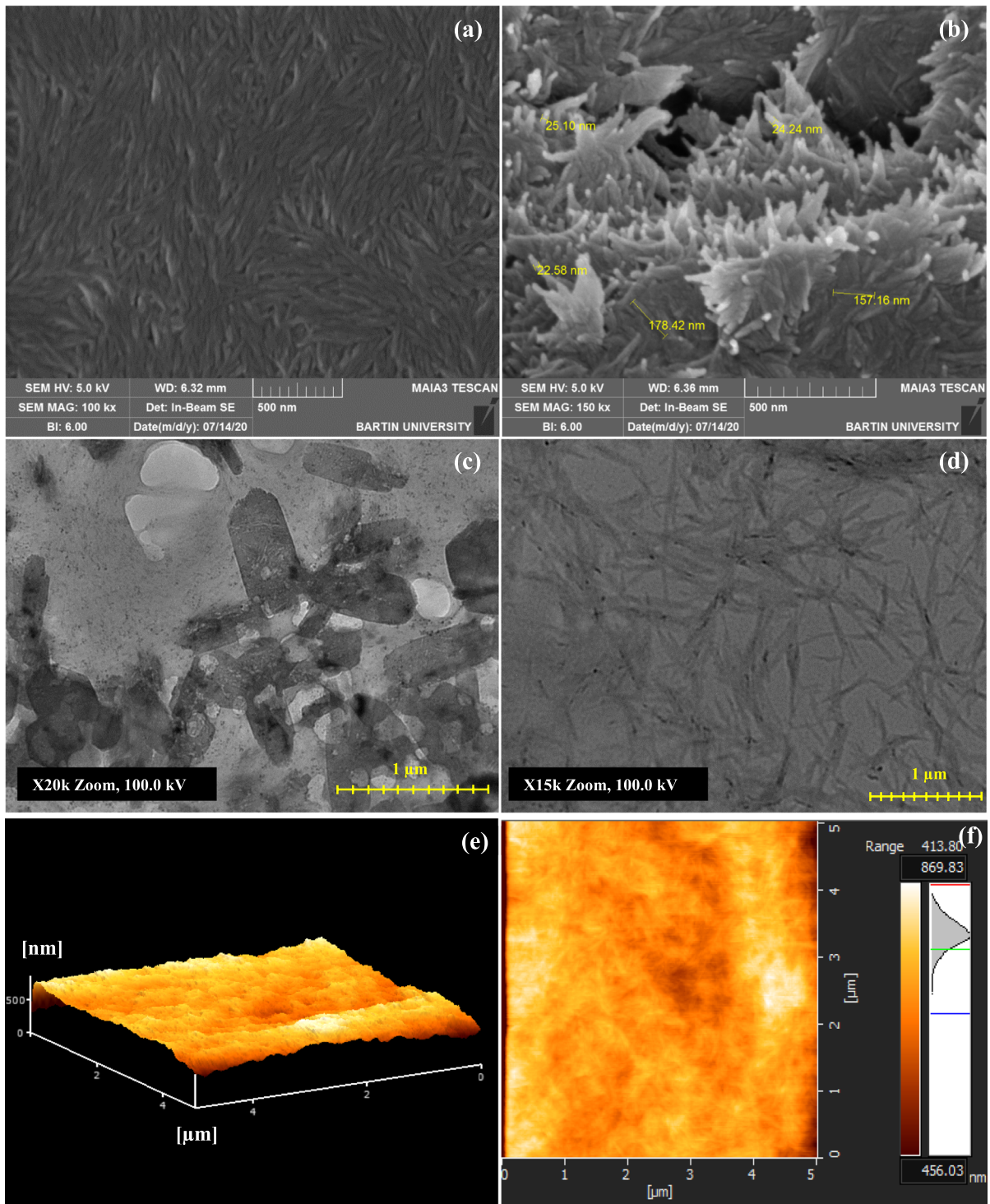


Fig. 3 SEM (a, b), TEM (c, d) and AFM (e, f) images of the CNCs

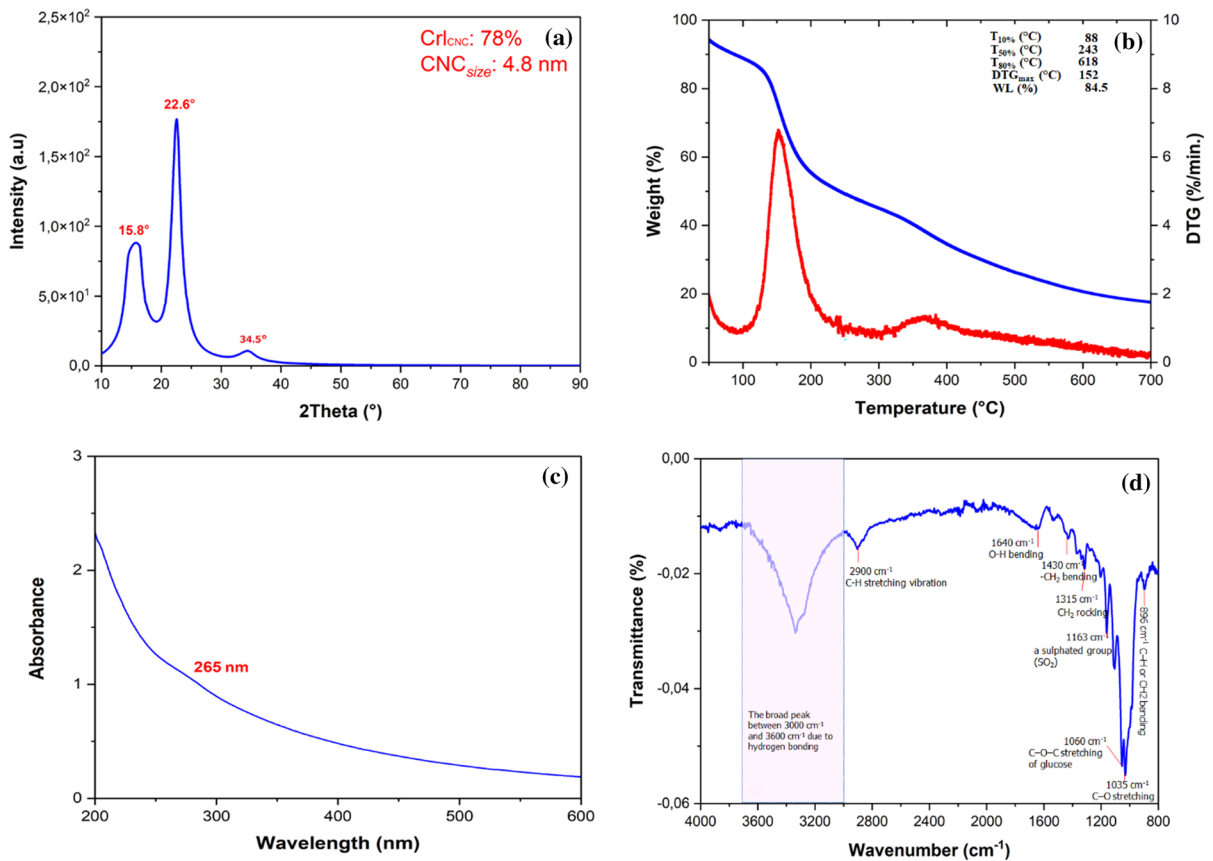


Fig. 4 XRD pattern (a), TG–DTA curves (b), UV–Vis curve (c), and FTIR spectra (d) of the cellulose nanocrystals

and 80% mass loss was found as 88 °C, 243 °C, and 618 °C, respectively. DTG curves showed a decomposition peak at 150–200 °C and the temperature occurred the maximum mass loss per unit time (DTG_{max}) was detected at 152 °C. After TG analysis, the weight loss of CNCs were calculated as 84.5%. In Fig. 4c, CNCs exhibited a weak absorbance at 265 nm. The previous studies determined an absorption at 260–290 nm (Sirviö et al. 2016), however; Yu et al. (2015) found that there were no obvious peaks in the UV–Vis spectrum of the CNCs. FTIR analysis from 800 to 4000 cm⁻¹ was conducted to investigate the chemical structure of CNCs as given in Fig. 4d. The broad peaks in the range of 3700–3000 cm⁻¹ can be related to stretching and bending vibrations of hydrogen bonding (Man et al. 2011; Azizi et al. 2013). C–H stretching vibration and CH₂ bending vibration appear around 2900 and 1430 cm⁻¹ (Man et al. 2011). The

peaks at around 1640 and 1060 cm⁻¹ can be attributed to the O–H bending of absorbed water (Lu and Hsieh 2010) and the C–O–C stretching of glucose ring skeletal vibration (Cherian et al. 2008; Yu et al. 2015). The peak at 1163 cm⁻¹ in the spectrum exhibit the presence of a sulfated group probably due to sulfonation of cellulose occurring during the acid hydrolysis process with sulphuric acid (Chieng et al. 2017). The peaks in the FTIR spectrum in Fig. 4d are seen at 1315, 1035, and 896 cm⁻¹, representing typical cellulose absorption peaks. These peaks can be defined as CH₂ rocking, C–O stretching, and C–H or CH₂ bending. The CNCs were mixed with PVDF–DMF solution and the nano-fibers at CNC loading rates from 0.25 to 1% were obtained with the electrospinning technique. Smooth-surfaced fibers were obtained for all solutions and all fibers were seed generally individually and homogeneously dispersed as seen in Fig. 5. The

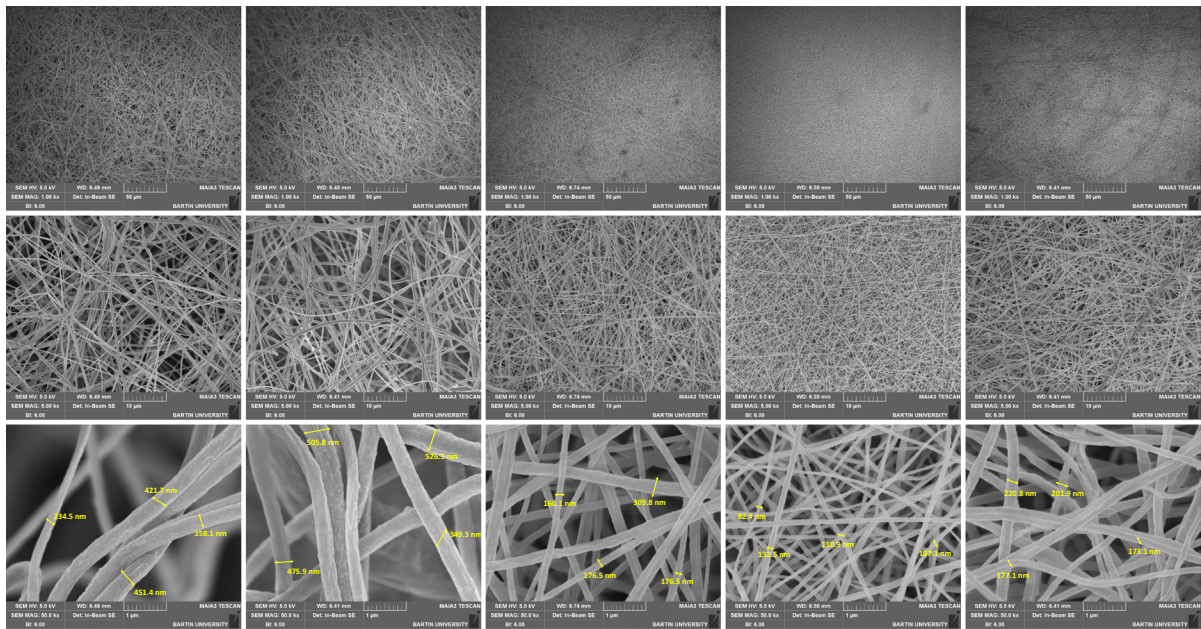


Fig. 5 SEM images of the PVDF nanofibers with CNCs obtained with the electrospinning technique (All images in the same line are the same magnitudes)

average diameters of the nanofibers were calculated from SEM images, using the Paint software (15–20 diameters per specimen). The fiber's diameters obtained from neat PVDF were found to generally range from 200 to 460 nm. While CNC loading rate ranged from 0.25 to 1%, the fiber's diameters generally decreased. These results revealed that neat PVDF nanofibers prepared without any loadings of CNCs were having an average fiber diameter of $(350 \pm 100 \text{ nm})$, while as, the average diameter of fibers prepared by the different loadings of 0.25%,

0.50%, 0.75%, and 1% of CNCs generally were having decreased average diameters of $(400 \pm 150 \text{ nm}$, $250 \pm 100 \text{ nm}$, $150 \pm 80 \text{ nm}$, and $150 \pm 100 \text{ nm})$, respectively. The largest and lowest fiber diameter was determined for the PVDF–0.25CNCs and the PVDF–0.75CNCs. In previous studies, the diameters of PVDF nanofibers with various loading rates of CNCs were seen to generally change from 50 to 900 nm in Table 1.

Table 1 The diameters of PVDF nanofibers with various loading rates of CNCs with electrospinning technique

CNCs in solution (%)	Solvent systems	Diameters (nm)	Sources
0.25–1	DMF	150–400	This study
0.5–1	DMAc	100–900	Gopi et al. (2018)
1	DMF	150–300	Mousa et al. (2022)
1	CHCl ₃ ; DMF (4:1)	300–650	Leonés et al. (2021)
1–5	DMF	718–559	Fashandi et al. (2016)
1–5	DMF	50–200	Ram et al. (2020)
2–6	DMF	400–900	Wang et al. (2019)
4	Acetone/DMF	370–870	Issa et al. (2016)
4–10	Acetone/DMF	150–300	Yan et al. (2022)
5–20	Acetone/DMF	250–750	Huan et al. (2018)

Table 2 Physical characterization of PVDF–CNC nanofiber mats

Samples	Grammage (g/m^2)	Thickness (μm)	Burst strength (kg/cm^2)	Air permeability (mL/min)	Fiber diameter (nm)
Neat PVDF	40 (± 5)	150 (± 13)	1.2 (± 0.1)	> 5000	350 (± 100)
PVDF–0.25CNCs	12 (± 1)	88 (± 7)	1.0 (± 0.1)	3635 (± 126)	400 (± 150)
PVDF–0.50CNCs	11 (± 2)	110 (± 12)	1.1 (± 0.1)	4790 (± 120)	250 (± 100)
PVDF–0.75CNCs	16 (± 1)	105 (± 5)	1.1 (± 0.1)	2380 (± 150)	150 (± 80)
PVDF–1CNCs	15 (± 3)	85 (± 5)	0,9 (± 0.1)	3150 (± 105)	150 (± 100)

Table 2 shows a physical characterization of PVDF–CNC nanofiber mats obtained with the electrospinning technique.

The nanofibers' grammage and thickness were calculated to range from 40 to 11 g/m^2 and from 150 to 85 μm , respectively as seen in Table 2. The burst strength for all samples was similar to each other. The

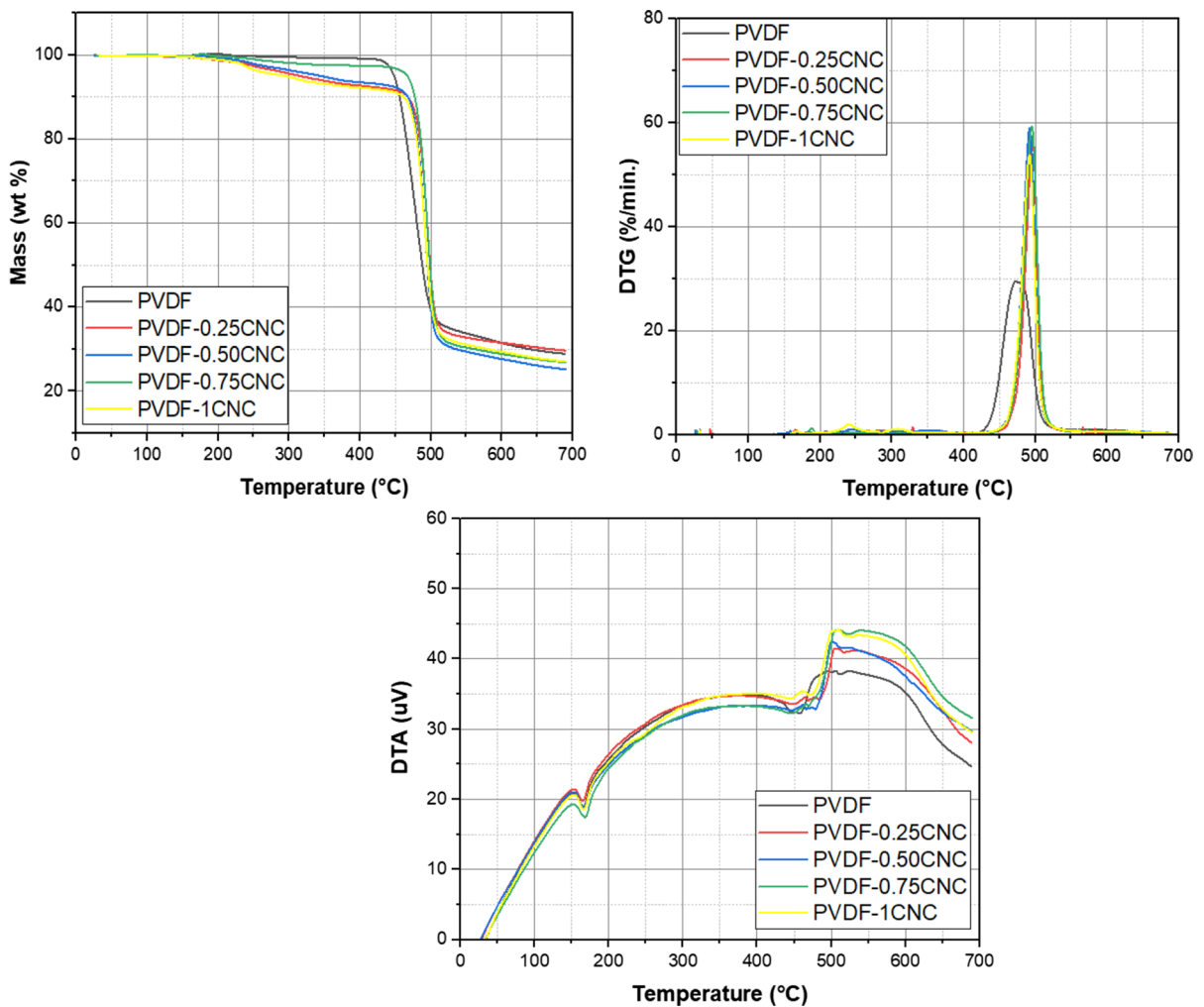
**Fig. 6** Thermogravimetric analysis of neat PVDF and the PVDF with CNC nanofibers

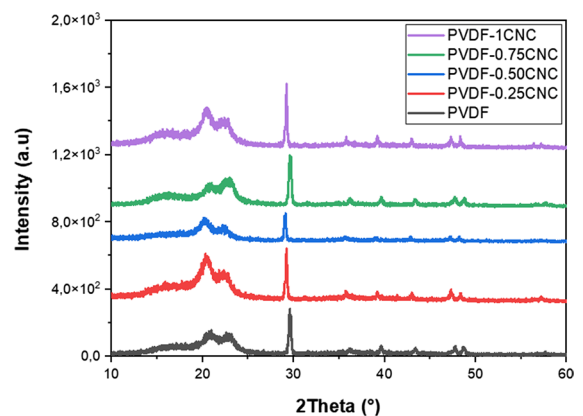
Table 3 Summary results of thermal analysis of neat PVDF and the PVDF with CNC nanofibers

Samples	T _{10%} (°C)	T _{50%} (°C)	DTG _{max} (°C)	WL (%)	T _m (°C)	T _d (°C)
PVDF	455.9	487.9	473.3	71.2	165.1	457.8
PVDF–0.25CNCs	467.7	498.6	495.9	70.4	164.7	469.5
PVDF–0.50CNCs	467.9	494.7	492.5	74.8	166.7	470.7
PVDF–0.75CNCs	477.4	498.7	495.3	73.1	168.3	469.6
PVDF–1CNCs	461.9	495.1	492.2	72.3	166.2	468.4

air permeability of the nano-fibers with CNCs was found to change between 2380 and 4790 mL/min, however, the air permeability for neat PVDF nanofibers could not be detected and the obtained results were generally above 5000 mL/min.

The thermal analysis of neat PVDF and PVDF with CNC nanofibers was conducted from 30 to 700 °C and the obtained TG curves are given in Fig. 6. Table 3 shows the summary of TG curves of CNCs. The thermal decomposition of neat PVDF and PVDF with CNC nanofibers consists of degradation peaks at different areas occurring between 200 and 700 °C. The DTG curves showed decomposition peaks of all samples at 450–500 °C as given in Fig. 6 due to hydrolysis, decomposition (at temperatures between 200 and 500 °C), and oxidative chain scission (at temperatures above 500 °C) of neat PVDF and PVDF with CNC nanofibers as exhibited from the DTG curves. DTA curves can provide the melting temperature (T_m) and degradation temperature (T_d) of the polymeric materials. According to the DTA results in Fig. 6, all T_m and T_d were similar to each other, and the T_m and T_d values of the samples ranged from 164.7 and 457.8 °C to 168.3 and 470.7 °C, respectively.

As seen in Table 3, T_{10%} and T_{50%} of neat PVDF increased with adding the CNCs. When CNC loading rates increased, T_{10%} and T_{50%} generally raised. T_{10%} and T_{50%} of the samples were found to change from 455.9 to 477.4 °C and from 487.9 to 498.7 °C, respectively. DTG_{max} of the PVDF with CNC nanofibers was found to be higher than neat PVDF nanofibers, and the highest and lowest DTG_{max} was found at 495.9 °C for the PVDF nanofibers with 0.25% CNCs and 473.3 °C for the neat PVDF nanofibers, respectively. T_m and T_d of the samples were determined to range from 164.7 to 168.3 °C and from 457.8 to 470.7 °C, respectively. The weight loss ranged from 70.4% (PVDF–0.25CNCs) to 74.8 °C (PVDF–0.50CNCs). As a result, it can be concluded

**Fig. 7** XRD analysis of neat PVDF and PVDF with CNC nanofibers**Table 4** Summary results of XRD analysis of neat PVDF and the PVDF with CNC nanofibers

Samples	2Theta (°)	Crystallinity index (%)	Crystal size (nm)
PVDF	20.8, 22.9, 29.6	64.0	20.2
PVDF–0.25CNCs	20.4, 22.4, 29.2	64.5	5.6
PVDF–0.50CNCs	20.2, 22.3, 29.1	65.0	5.1
PVDF–0.75CNCs	20.7, 22.9, 29.6	66.0	4.8
PVDF–1CNCs	20.4, 22.4, 29.2	65.5	4.9

that the addition of CNCs generally improved the thermal stability of neat PVDF.

Figure 7 shows the XRD pattern graphs of neat PVDF and the PVDF nanofibers with CNCs. Neat PVDF and its nanofibers with CNCs were exhibited at three main peaks at around 20°, 22°, and 29° in the XRD graph. Although the addition of CNCs slightly decreased the 2θ degree of neat PVDF, all XRD patterns were generally similar to each other. According to the XRD, the crystallinity of the neat PVDF and its nanofibers with CNCs were

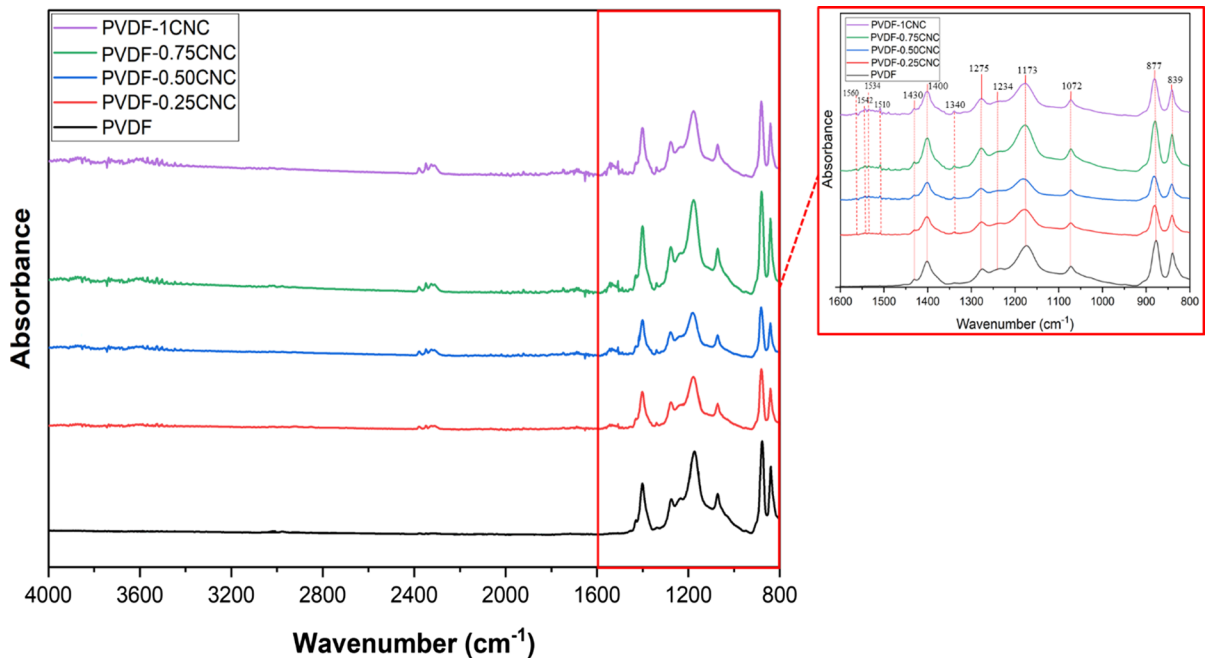


Fig. 8 FTIR analysis of neat PVDF and the PVDF with CNC nanofibers

calculated as seen in Table 4. The crystallinity was found to range from 64 to 66%.

FTIR analysis of the neat PVDF and the PVDF with CNC nanofibers was conducted from 800 to 4000 cm^{-1} as given in Fig. 8.

The FTIR spectra of PVDF were detected at seven characteristic peaks including 840 cm^{-1} , 873 cm^{-1} , 1070 cm^{-1} , 1172 cm^{-1} , 1234 cm^{-1} , 1275 cm^{-1} , 1401 cm^{-1} , 1431 cm^{-1} (Zeng et al. 2016; Tao et al. 2012; Medeiros et al. 2018) because of three crystalline phases including three phases γ , α , and β according to the literature. The FTIR spectra were at 1233 cm^{-1} due to the γ -phase, at 838, 1072, and 1170 cm^{-1} due to the β -phase, and at 876 cm^{-1} and 1402 cm^{-1} due to the α -phase. The obtained FTIR spectra in this study were generally similar to previous studies (Zeng et al. 2016; Tao et al. 2012; Medeiros et al. 2018), and also the wavenumbers belonging to the CNCs were detected at 1340 cm^{-1} , 1510 cm^{-1} , 1534 cm^{-1} , 1542 cm^{-1} , and 1560 cm^{-1} . As a result, it can be said that there is no difference in FTIR spectra of PVDF–CNC nanofibers.

Conclusions

CNCs were obtained from MCC with acid hydrolysis and the PVDF with CNCs nanofibers at low loading rates of 0.25, 0.5, 0.75, and 1% were successfully prepared with the electrospinning technique. The results showed that when the loading rates of CNCs were raised from 0.25 to 1%, adding CNCs to PVDF generally decreased the obtained fiber diameters. The presence of CNCs in PVDF improved the thermal stability of the PVDF nanofibers and thermal degradation temperature including $T_{10\%}$, $T_{50\%}$, and DTG_{\max} increased with the addition of CNCs, however weight loss increased with the presence of CNCs. XRD results showed that crystallinity generally increased with adding CNCs and when the loading rate of CNCs was raised, the crystallinity of the nanofibers generally was higher than neat PVDF nanofibers. In FTIR spectra, the chemical structure of the samples exhibited the seven characteristic peaks belonging to PVDF and CNCs, and any difference was not detected among the FTIR spectra of the PVDF–CNC nanofibers. As a result, it can be concluded that the

addition of CNCs generally improved the properties of neat PVDF nanofibers.

Acknowledgments We also would like to acknowledge Inovenso Co. Ltd. for the electrospinning device as a courtesy.

Author contributions I declare that all the authors had significant participation in the development of this work. DA, ES, GG: wrote the manuscript text, IB: prepared electrospinning fibers, and EC, SKG, AK-P, and TB: produced cellulose nanocrystals. All authors reviewed the manuscript.

Funding The study was supported by the department of scientific research project coordination (BAP) of Bartın University (Project Number: 2018-FEN-A-009).

Availability of data and materials Not applicable.

Declarations

Competing interests The authors declare no competing interests.

Conflict of interest The authors declare that they have no known conflict of interests or personal relationships.

Ethics approval and consent to participate Not applicable.

Consent for publication Not applicable.

References

- Akduman C (2021) Cellulose acetate and polyvinylidene fluoride nanofiber mats for N95 respirators. *J Ind Text* 50(8):1239–1261
- Alhassan ZA, Burezq YS, Nair R et al (2018) Polyvinylidene difluoride piezoelectric electrospun nanofibers: review in synthesis, fabrication, characterizations, and applications. *J Nanomater*. <https://doi.org/10.1155/2018/8164185>
- Aydemir D, Gardner DJ (2020a) Biopolymer blends of polyhydroxybutyrate and polylactic acid reinforced with cellulose nanofibrils. *Carbohydr Polym* 250:116867. <https://doi.org/10.1016/j.carbpol.2020.116867>
- Aydemir D, Gardner DJ (2020b) The effects of cellulosic fillers on the mechanical, morphological, thermal, viscoelastic, and rheological properties of polyhydroxybutyrate biopolymers. *Polym Compos* 41(9):3842–3856. <https://doi.org/10.1002/pc.25681>
- Azizi S, Ahmad M, Mahdavi M et al (2013) Preparation, characterization, and antimicrobial activities of ZnO nanoparticles/cellulose nanocrystal nanocomposites. *BioResources* 8(2):1841–1851
- Bondeson D, Mathew A, Oksman K (2006) Optimization of the isolation of nanocrystals from microcrystalline cellulose by acid hydrolysis. *Cellulose* 13(2):171–180. <https://doi.org/10.1007/s10570-006-9061-4>
- Cherian BM, Pothan LA, Nguyen-Chung T et al (2008) A novel method for the synthesis of cellulose nanofibril whiskers from banana fibers and characterization. *J Agric Food Chem* 56(14):5617–5627. <https://doi.org/10.1021/jf8003674>
- Chieng BW, Lee SH, Ibrahim NA et al (2017) Isolation and characterization of cellulose nanocrystals from oil palm mesocarp fiber. *Polymers* 9(8):355. <https://doi.org/10.3390/polym9080355>
- Damaraju SM, Wu S, Jaffe M et al (2013) Structural changes in PVDF fibers due to electrospinning and its effect on biological function. *Biomed Mater* 8:045007. <https://doi.org/10.1088/1748-6041/8/4/045007>
- Dodds JS, Meyers FN, Loh KJ et al (2012) Piezoelectric characterization of PVDF-TrFE thin films enhanced with ZnO nanoparticles. *IEEE Sens J* 12:1889–1890. <https://doi.org/10.1109/JSEN.2011.2182043>
- Fashandi H, Abolhasani MM, Sandoghdar P et al (2016) Morphological changes towards enhancing piezoelectric properties of PVDF electrical generators using cellulose nanocrystals. *Cellulose* 23(6):3625–3637. <https://doi.org/10.1007/s10570-016-1070-3>
- Fu R, Chen S, Lin Y et al (2017) Improved piezoelectric properties of electrospun poly(vinylidene fluoride) fibers blended with cellulose nanocrystals. *Mater Lett* 187:86–88. <https://doi.org/10.1016/j.matlet.2016.10.068>
- Gopi S, Kargl R, Kleinschek KS et al (2018) Chitin nanowhisker-inspired electrospun PVDF membrane for enhanced oil–water separation. *J Environ Manag* 228:249–259. <https://doi.org/10.1016/j.jenvman.2018.09.039>
- Huan S, Liu G, Cheng W et al (2018) Electrospun poly(lactic acid)-based fibrous nanocomposite reinforced by cellulose nanocrystals: impact of fiber uniaxial alignment on microstructure and mechanical properties. *Biomacromolecules* 19(3):1037–1046. <https://doi.org/10.1021/acs.biomac.8b00023>
- Huang Z-M, Zhang Y-Z, Kotaki M et al (2003) Review on polymer nanofibers by electrospinning and their applications in nanocomposites. *Compos Sci Technol* 63:2223–2253. [https://doi.org/10.1016/S0266-3538\(03\)00178-7](https://doi.org/10.1016/S0266-3538(03)00178-7)
- Issa AA, Al-Maadeed M, Luyt AS et al (2016) Investigation of the physico-mechanical properties of electrospun PVDF/cellulose (nano) fibers. *J Appl Polym Sci* 133(26):43594. <https://doi.org/10.1002/app.43594>
- Kalia SA, Dufresne BM, Cherian BS et al (2011) Cellulose-based bio-and nanocomposites: a review. *Int J Polym Sci* 2011:1–35. <https://doi.org/10.1016/B978-0-08-100957-4.00013-9>
- Katta P, Alessandro M, Ramsier R et al (2004) Continuous electrospinning of aligned polymer nanofibers onto a wire drum collector. *Nano Lett* 4:2215–2218. <https://doi.org/10.1021/nl0486158>
- Lee JE, Shin YE, Lee GH et al (2021) Polyvinylidene fluoride (PVDF)/cellulose nanocrystal (CNC) nanocomposite fiber and triboelectric textile sensors. *Compos Part B Eng* 223:109098. <https://doi.org/10.1016/j.compositesb.2021.109098>
- Leonés A, Salaris V, Mujica-Garcia A (2021) PLA electrospun fibers reinforced with organic and

- inorganic nanoparticles: a comparative study. *Molecules* 26(16):4925. <https://doi.org/10.3390/molecules26164925>
- Li Y, Wang B, Ma M et al (2018) The influence of pre-treatment time and sulfuric acid on cellulose nanocrystals. *BioResourse* 13(2):3585–3602
- Lolla D, Pan L, Gade H et al (2018) Functionalized polyvinylidene fluoride electrospun nanofibers and applications. In: Tomasz T, Pawel J, Wiktor M (eds) *Electrospinning method used to create functional nanocomposites films*. IntechOpen, London, pp 69–89. <https://doi.org/10.5772/intechopen.76261>
- Lu P, Hsieh Y-L (2010) Preparation and properties of cellulose nanocrystals: rods, spheres, and network. *Carbohydr Polym* 82:329–336. <https://doi.org/10.1016/j.carbpol.2010.04.073>
- Mago G, Kalyon DM, Fisher FT (2008) Membranes of polyvinylidene fluoride and PVDF nanocomposites with carbon nanotubes via immersion precipitation. *J Nanomater*. <https://doi.org/10.1155/2008/759825>
- Man Z, Muhammad N, Sarwono A et al (2011) Preparation of cellulose nanocrystals using an ionic liquid. *J Polym Environ* 19(3):726–731. <https://doi.org/10.1007/s10924-011-0323-3>
- Martin B, Dantras E, Lonjon A et al (2019) Fabrication of nickel nanochains/PVDF nanocomposites and their electrical/magnetic properties. *Phys Status Solidi (a)* 216(16):1900158
- Medeiros KAR, Rangel EQ, Sant'Anna AR et al (2018) Evaluation of the electromechanical behavior of polyvinylidene fluoride used as a component of risers in the offshore oil industry. *Oil Gas Sci Technol-Rev d'IFP Energ nouv* 73:48. <https://doi.org/10.2516/ogst/2018058>
- Mokhtari F, Latifi M, Shamshirsaz M (2016) Electrospinning/electrospray of polyvinylidene fluoride (PVDF): piezoelectric nanofibers. *J Text Inst* 107(8):1037–1055. <https://doi.org/10.1080/00405000.2015.1083300>
- Mousa HM, Fahmy HS, Abouzeid R et al (2022) Polyvinylidene fluoride-cellulose nanocrystals hybrid nanofiber membrane for energy harvesting and oil–water separation applications. *Mater Lett* 306:130965. <https://doi.org/10.1016/j.matlet.2021.130965>
- Ram F, Gudadhe A, Vijayakanth T et al (2020) Nanocellulose reinforced flexible composite nanogenerators with enhanced vibrational energy harvesting and sensing properties. *ACS Appl Polym Mater* 2(7):2550–2562. <https://doi.org/10.1021/acscpm.0c00158>
- Reddy JP, Rhim JW (2014) Isolation and characterization of cellulose nanocrystals from garlic skin. *Mater Lett* 129:20–23. <https://doi.org/10.1016/j.matlet.2014.05.019>
- Reneker DH, Yarin AL, Fong H et al (2000) Bending instability of electrically charged liquid jets of polymer solutions in electrospinning. *J Appl Phys* 87(9):4531–4547. <https://doi.org/10.1063/1.373532>
- Rincón-Iglesias M, Lizundia E, Correia DM et al (2020) The role of CNC surface modification on the structural, thermal and electrical properties of poly (vinylidene fluoride) nanocomposites. *Cellulose* 27(7):3821–3834. <https://doi.org/10.1007/s10570-020-03067-z>
- Sanders JE, Han Y, Rushing TS (2019) Electrospinning of cellulose nanocrystal-filled poly (Vinyl alcohol) solutions: material property assessment. *Nanomaterials* 9(5):805. <https://doi.org/10.3390/nano9050805>
- Shaheen TI, Emam HE (2018) Sono-chemical synthesis of cellulose nanocrystals from wood sawdust using acid hydrolysis. *Int J Biol Macromol* 107:1599–1606. <https://doi.org/10.1016/j.ijbiomac.2017.10.028>
- Sheikh FA, Cantu T, Macossay J (2011) Fabrication of poly (vinylidene fluoride) (PVDF) nanofibers containing nickel nanoparticles as future energy server materials. *Sci Adv Mater* 3(2):216–222. <https://doi.org/10.1166/sam.2011.1148>
- Sheikh FA, Beigh MA, Qadir AS et al (2019) Hydrophilically modified poly (vinylidene fluoride) nanofibers incorporating cellulose acetate fabricated by colloidal electrospinning for future tissue-regeneration applications. *Polym Compos* 40(4):1619–1630. <https://doi.org/10.1002/pc.24910>
- Sirviö JA, Visanko M, Heiskanen JP (2016) UV-absorbing cellulose nanocrystals as functional reinforcing fillers in polymer nanocomposite films. *J Mater Chem A* 4(17):6368–6375. <https://doi.org/10.1039/C6TA00900J>
- Swamidoss FV, Bangaru M, Nalathambi G et al (2019) Silver-incorporated polyvinylidene fluoride nanofibers for bacterial filtration. *Aerosol Sci Technol* 53(2):196–206. <https://doi.org/10.1080/02786826.2018.1554892>
- Tao M, Liu F, Xue L (2012) Hydrophilic poly (vinylidene fluoride) (PVDF) membrane by in situ polymerization of 2-hydroxyethyl methacrylate (HEMA) and micro-phase separation. *J Mater Chem* 22(18):9131–9137. <https://doi.org/10.1039/C2JM30695F>
- Victor FS, Kugarajah V, Bangaru M et al (2021) Electrospun nanofibers of polyvinylidene fluoride incorporated with titanium nanotubes for purifying the air from bacterial contamination. *Environ Sci Pollut Res* 28:1–14
- Wang X, Cheng W, Wang D et al (2019) Electrospun polyvinylidene fluoride-based fibrous nanocomposite membranes reinforced by cellulose nanocrystals for efficient separation of water-in-oil emulsions. *J Membr Sci* 575:71–79. <https://doi.org/10.1016/j.memsci.2018.12.057>
- Xin Y, Zhu J, Sun H et al (2018) A brief review on piezoelectric PVDF nanofibers prepared by electrospinning. *Ferroelectrics* 526(1):140–151. <https://doi.org/10.1080/00150193.2018.1456304>
- Yan J, Bai T, Yue Y et al (2022) Nanostructured superior oil-adsorbent nanofiber composites using one-step electrospinning of polyvinylidene fluoride/nanocellulose. *Compos Sci Technol* 224:109490. <https://doi.org/10.1016/j.compscitech.2022.109490>
- Yarin A, Kataphinan W, Reneker DH (2005) Branching in electrospinning of nanofibers. *J Appl Phys* 98:064501. <https://doi.org/10.1063/1.2060928>
- Yee WA, Kotaki M, Liu Y et al (2007) Morphology, polymorphism behavior and molecular orientation of electrospun poly(vinylidene fluoride) fibers. *Polymer* 48(2):512–521. <https://doi.org/10.1016/j.polymer.2006.11.036>
- Yu HY, Chen GY, Wang YB et al (2015) A facile one-pot route for preparing cellulose nanocrystal/zinc oxide nanohybrids with high antibacterial and photocatalytic activity. *Cellulose* 22(1):261–273. <https://doi.org/10.1007/s10570-014-0491-0>

- Zeng Z, Yu D, He Z et al (2016) Graphene oxide quantum dots covalently functionalized PVDF membrane with significantly enhanced bactericidal and anti-biofouling performances. *Sci Rep* 6(1):1–11. <https://doi.org/10.1038/srep20142>
- Zeng J, Wang H, Chen X et al (2021) Fabrication of polyvinylidene fluoride/silver nanofiber membrane with antibacterial and anti-yellowing properties. *AIP Adv* 11(7):075310. <https://doi.org/10.1063/5.0038173>
- Zhang Z, Wu Q, Song K et al (2015) Poly (vinylidene fluoride)/cellulose nanocrystals composites: rheological, hydrophilicity, thermal, and mechanical properties. *Cellulose* 22(4):2431–2441. <https://doi.org/10.1007/s10570-015-0634-y>

Publisher's Note Springer Nature remains neutral with regard to jurisdictional claims in published maps and institutional affiliations.

Springer Nature or its licensor (e.g. a society or other partner) holds exclusive rights to this article under a publishing agreement with the author(s) or other rightsholder(s); author self-archiving of the accepted manuscript version of this article is solely governed by the terms of such publishing agreement and applicable law.